



HAL
open science

The pathogenic MT-ATP6 m.8851T>C mutation prevents proton movements within the n-side hydrophilic cleft of the membrane domain of ATP synthase

Alain Dautant, Roza Kucharczyk, Kewin Gombeau, François Godard, Déborah Tribouillard-Tanvier, Jean-Paul Di Rago

► To cite this version:

Alain Dautant, Roza Kucharczyk, Kewin Gombeau, François Godard, Déborah Tribouillard-Tanvier, et al.. The pathogenic MT-ATP6 m.8851T>C mutation prevents proton movements within the n-side hydrophilic cleft of the membrane domain of ATP synthase. *Biochimica biophysica acta (BBA) - Bioenergetics*, 2019, 1860 (7), pp.562-572. 10.1016/j.bbabo.2019.06.002 . hal-02988559

HAL Id: hal-02988559

<https://cnrs.hal.science/hal-02988559>

Submitted on 25 Oct 2021

HAL is a multi-disciplinary open access archive for the deposit and dissemination of scientific research documents, whether they are published or not. The documents may come from teaching and research institutions in France or abroad, or from public or private research centers.

L'archive ouverte pluridisciplinaire **HAL**, est destinée au dépôt et à la diffusion de documents scientifiques de niveau recherche, publiés ou non, émanant des établissements d'enseignement et de recherche français ou étrangers, des laboratoires publics ou privés.



Distributed under a Creative Commons Attribution - NonCommercial 4.0 International License

The pathogenic *MT-ATP6* m.8851T>C mutation prevents proton movements within the *n*-side hydrophilic cleft of the membrane domain of ATP synthase

Roza Kucharczyk^{1, 2, a, *}, Alain Dautant^{1, a}, Kewin Gombeau¹, François Godard¹, Déborah Tribouillard-Tanvier^{1, §}, and Jean-Paul di Rago^{1, *}

¹ Institut de Biochimie et Génétique Cellulaires of CNRS, Bordeaux University, 1 Rue Camille Saint-Saëns, Bordeaux 33077 cedex, France.

² Institute of Biochemistry and Biophysics, Polish Academy of Sciences, Warsaw, Poland

^a These authors equally contributed to this work

[§] Research Associate from INSERM

*To whom correspondence should be addressed. Email : jp.dirago@ibgc.cnrs.fr or roza@ibb.waw.pl

Abstract

1
2 Dozens of pathogenic mutations have been localized in the mitochondrial gene (*MT-ATP6*) that
3 encodes the subunit *a* of ATP synthase. The subunit *a* together with a ring of identical subunits *c*
4 moves protons across the mitochondrial inner membrane coupled to rotation of the subunit *c*-ring and
5 ATP synthesis. One of these mutations, m.8851T>C, has been associated with bilateral striatal lesions
6 of childhood (BSLC), a group of rare neurological disorders characterized by symmetric degeneration
7 of the corpus striatum. It converts a highly conserved tryptophan residue into arginine at position 109
8 of subunit *a* (*aW*₁₀₉R). We previously showed that an equivalent thereof in *Saccharomyces cerevisiae*
9 (*aW*₁₂₆R) severely impairs by an unknown mechanism the functioning of ATP synthase without any
10 visible assembly/stability defect. Herein we show that ATP synthase function was recovered to
11 varying degree by replacing the mutant arginine residue 126 with methionine, lysine or glycine or by
12 replacing with methionine an arginine residue present in position 169 of subunit *a* (*aR*₁₆₉). In recently
13 described atomic structures of yeast ATP synthase, *aR*₁₆₉ is at the center of an hydrophilic cleft along
14 which protons are transported from the subunit *c*-ring to the mitochondrial matrix, in the proximity of
15 the two residues known from a long time to be essential to the activity of F_O (*aR*₁₇₆ and *cE*₅₉). We
16 provide evidence that the *aW*₁₂₆R change is responsible for an electrostatic and steric hindrance that
17 enables *aR*₁₆₉ to engage in a salt bridge with *cE*₅₉. As a result, *aR*₁₇₆ cannot interact properly with *cE*₅₉
18 and ATP synthase fails to effectively move protons across the mitochondrial membrane. In addition to
19 insight into the pathogenic mechanism induced by the m.8851T>C mutation, the present study brings
20 interesting information on the role of specific residues of subunit *a* in the energy-transducing activity
21 of ATP synthase.

22

23 **Introduction**

24 Mitochondria provide aerobic eukaryotes with cellular ATP through the process of oxidative
25 phosphorylation (OXPHOS) [1]. In this process electrons released by the oxidation of fatty acids and
26 carbohydrates are shuttled to oxygen by four complexes (I–IV) embedded in the mitochondrial inner
27 membrane and protons are concomitantly transported from the mitochondrial matrix into the space
28 between the two membranes that surround the organelle. Protons are returned back to the matrix by
29 ATP synthase (complex V), which is coupled to ATP synthesis from ADP and inorganic phosphate [2].
30 The ATP synthase organizes into a membrane-embedded domain (F_0) and a membrane-extrinsic
31 catalytic sector (F_1) [3-5]. Within the F_0 , protons are transported by the subunit *a* and a ring of
32 identical *c* subunits (8 in mammals, 10 in yeast [6]), which leads to rotation of the subunit *c*-ring and
33 conformational changes in the F_1 that favor the synthesis of ATP and its release into the mitochondrial
34 matrix.

35 Considerable progress towards a molecular description of the energy-transducing mechanism
36 of ATP synthase has been achieved recently with the resolution of complete atomic structures of this
37 enzyme [4, 7-9]. Evaluating the role of specific amino acid residues in these structures requires a
38 genetically approachable system where nuclear and mitochondrial genes can be modified because of
39 the mixed genetic origin of ATP synthase in the vast majority of eukaryotes. Baker's yeast
40 *Saccharomyces cerevisiae* is by far the most convenient [10]. The incapacity of cells from this
41 unicellular fungus to stably maintain the co-existence of different mitochondrial DNA molecules
42 (heteroplasmy) is especially helpful to investigate in isolation the functional consequences of specific
43 mutations of this DNA [11]. Another major advantage is the good fermenting capacity of *S. cerevisiae*,
44 which enables survival to mutations that inactivate oxidative phosphorylation.

45 We have exploited these attributes to investigate the biochemical consequences of pathogenic
46 amino acid replacements in subunit *a* induced by mutations in the mitochondrial *MT-ATP6* gene [12-
47 18]. With yeast strains homoplasmic for equivalents of these mutations it was possible to evaluate
48 more precisely their impact on ATP synthase than with patient's cells and tissues where they generally
49 co-exist with wild type mtDNA (heteroplasmy). In all cases a substantial lack of mitochondrial ATP
50 production, ranging from 30 to >90%, was observed in correlation with the severity of the clinical

51 phenotypes induced by these mutations. Although interesting, these observations provide limited
52 information because detrimental amino acid changes may affect residues that have minor if any
53 functional importance. However, one can take advantage of loss-of-function mutations to seek for
54 genetic reversions that lead to function regain without recovering the wild type structure of subunit *a*,
55 an approach that proved to be highly informative on several occasions. For instance, we recently
56 provided in this way evidence that a pathogenic serine-to-asparagine change at position 165 of yeast
57 subunit *a* (148 in humans) prevents the transport of protons from the subunit *c*-ring to the
58 mitochondrial matrix [18] not because the mutated serine is directly involved in proton conduction but
59 because its replacement by asparagine leads to the establishment of hydrogen bonds with a nearby
60 glutamate residue (*aE*₁₆₂) that is important for moving protons through the F_0 [19].

61 We herein applied this suppressor genetics approach to the m.8851T>C mutation that has been
62 associated to bilateral striatal lesions of childhood (BSLC), a group of rare neurological disorders
63 characterized by symmetric degeneration of the corpus striatum [20]. This mutation leads to
64 replacement of a highly conserved tryptophan residue with arginine at position 109 of human subunit
65 *a* (*aW*₁₀₉R). An equivalent thereof (*aW*₁₂₆R) very severely compromises the ability of yeast to
66 proliferate from non-fermentable substrates (e.g. glycerol, ethanol, or lactate) owing to defects in the
67 functioning of F_0 without any visible impact on the assembly/stability of ATP synthase [15]. We here
68 report that ATP synthase function was recovered to varying degrees by replacing the mutant arginine
69 residue 126 with methionine, lysine or glycine or by replacing with methionine an arginine residue
70 present in position 169 of subunit *a* (*aR*₁₆₉). The results provide evidence that the m.8851T>C
71 mutation impairs the movement of protons from the subunit *c*-ring towards the mitochondrial matrix
72 owing to electrostatic and steric hindrance with residues essential to the activity of F_0 [7, 21].

73

74

75

76 2. Materials and Methods

77 2.1. Growth media

78 The media used for growing yeast were: YPGA (1% Bacto yeast extract, 1% Bacto Peptone, 2% or 10%
79 glucose, 40 mg/L adenine); YPGalA (1% Bacto yeast extract, 1% Bacto Peptone, 2% galactose, 40
80 mg/L adenine); YPEGA (1% Bacto yeast extract, 1% Bacto Peptone, 3% ethanol, 2% glycerol, 40
81 mg/L adenine); W0 (2% glucose, 0.67% Nitrogen base with ammonium sulfate from Difco).
82 Sporulation was induced in SP1 medium: 0.1% glucose, 0.25% yeast extract, and 50 mM potassium
83 acetate. Solid media were obtained by adding 2% Bacto Agar (Difco, Becton Dickinson).

84

85 2.2. Selection of revertants from strain RKY39 (*aW_{126R}*).

86 The strain RKY39 (*MATa ade2-1 his3-11,15 trp1-1 leu2-3,112 ura3-1 CAN1 arg8::HIS3 [ρ^+ atp6-*
87 *W_{126R}]*) that carries an equivalent of the m.8851T>C (*aW_{126R}*) mutation [15] was subcloned on rich
88 2% glucose plates. Forty subclones were picked up and individually grown for three days in 10%
89 glucose. Glucose was removed from the cultures by two washings with water and 10^8 cells from each
90 culture were spread on rich glycerol/ethanol (YPEGA) plates. The plates were incubated at 28°C for at
91 least fifteen days. Only one revertant per plate was retained for further analysis to ensure genetic
92 independence of the isolates. The revertants were genetically purified by subcloning on glucose plates
93 and their *ATP6* gene was PCR-amplified with primers 5'TAATATACGGGGGTGGGTCCCTCAC
94 and 5'GGGCCGAAGTCCGAAGGAGTAAG and entirely sequenced.

95

96 2.3 *Epifluorescence Microscopy*. Epifluorescence microscopy of 4',6-diamidino-2-phenylindole
97 (DAPI)-stained and MitoTracker-Red CMXRos-stained cells was carried out with a Zeiss AxioImager
98 A2 microscope fitted with a $\times 100$ immersion objective and a standard FITC filter. Briefly, 3mL of
99 log-phase culture were incubated with DAPI ($5\mu\text{g}\cdot\text{mL}^{-1}$) and Mitotracker CMX ROS ($1\mu\text{g}\cdot\text{mL}^{-1}$) for
100 10min at 28°C with agitation. Then, cells were washed with 10mL of minimal media to remove the
101 excess of flurochrome, centrifugated and resuspended in 100 μL of minimal media prior to be
102 observed.

103

104 *Yeast RNA preparation and quantitative real-time PCR assay.* For each condition, a cellular
105 equivalent of 5 OD_{600nm} was sampled in log-phase culture grown for 8h in rich galactose media and
106 quick frozen to be further processed for total RNA extraction. To this aim, the Absolutely RNA
107 Miniprep kit (Agilent, Stratagene) was used, according to the manufacturer's instructions with the
108 following modification: to 300 µL of the lysis buffer containing guanidine thiocyanate and 2.1 µL β-
109 mercaptoethanol were subsequently added an equal volume of glass beads (Ø 0.5 mm) and an equal
110 volume of phenol:chloroform:isoamyl alcohol (25:24:1). Cells were then disrupted by vortexing 5
111 times for 30 seconds with station of 30 seconds in ice between each vortex session to avoid excessive
112 warming. The elution volume was 30 µL and the concentration of RNA was quantified using a
113 nanodrop spectrometer (NanoDrop 1000, Thermo Scientific). RNA purity was checked and met the
114 following requirements: A260/A280 >1.7 and A260/A230 >1.5. The integrity of the 18 and 26S
115 ribosomal bands was checked on a 1% agarose gel. First-strand cDNA was synthesized from 500 ng
116 total RNAs using the Affinity script QPCR cDNA synthesis kit (Agilent, Stratagene) according to the
117 manufacturer's instructions. The retro-transcription was performed by incubating the reactions at 25°C
118 for 5 min, 42°C for 45 min, and 95°C for 5 min. Specific primer pairs were determined using Primer-
119 BLAST software [22] and matched the coding sequence of the target genes. The GenBank accession
120 numbers and the corresponding primer pairs are summarised in Table S1. Real-time qPCR reactions
121 were performed using a Mx3000P QPCR System (Agilent, Stratagene) and the Brilliant III Ultra-Fast
122 SYBR® Green QPCR Master Mix with Low ROX (Agilent, Stratagene) according to the
123 manufacturer's instructions. The programme used was: one cycle at 95°C for 3 min and then 40
124 amplification cycles at 95°C for 20 sec and 60°C for 20 sec. For each sample, the level of expression
125 of the target gene was compared to the expression of the stably expressed *TFC6*, *TFB1* and *RMD8*
126 genes. That relative expression (REX) of the target gene was calculated according to the formula REX
127 = $\text{MEAN}[(E_{TFC6})^{Ct-TFC6} + (E_{TFB1})^{Ct-TFB1} + (E_{RMD8})^{Ct-RMD8}] / (E_{target})^{Ct-target}$. Ct is the number of PCR cycles
128 needed to enter in exponential phase of amplification; E is the amplification efficiency of couples of
129 primers specific to the reference and target genes, respectively. For each gene, the mean value of the
130 relative expression level, and the associated standard error ($n = 3$) were determined. Standard curves
131 were generated using 10-fold dilutions of a cDNA template on the Mx3000P apparatus, and using

132 each couple of gene specific primers (one standard curve per couple). Each dilution was assayed in
133 duplicate for each couple of primers. The reaction specificity was determined for each reaction from
134 the dissociation curve of the PCR product. This dissociation curve was obtained by following the
135 SybrGreen fluorescence level during a gradual heating of the PCR products from 55 to 95°C. Samples
136 were run in duplicate in optically clear 96-well plates (Agilent, Stratagene). All qPCR experiments
137 were performed according to the MIQE (Minimum Information for publication of Quantitative real-
138 time PCR Experiments) guidelines [23]. Each standard curve was made by plotting the Ct against the
139 log of the starting quantity of template for each dilution. The equation for the regression line and the r-
140 value was calculated. From that equation the slope of the standard curve was deduced and used to
141 calculate the PCR efficiency, E, for each couple of primers, as follows: $E = 10^{-1/\text{slope}}$. The measured
142 hybridization efficiencies were 1.85, 1.92, 1.89, 1.84 and 1.83 for *TFC6*, *TFB1*, *RMD8*, *COX2* and
143 *ATP8* genes, respectively.

144

145 *2.4 Quantification of mitochondrial DNA copy number per cell.* Measurement of mitochondrial DNA
146 copy number was determined using a previously described method [24]. For each condition, a
147 cellular equivalent of 1 OD_{600nm} was sampled in log-phase culture grown for 8h in rich galactose
148 media and quick frozen to be further processed for total DNA extraction. Total DNA was extracted
149 as described in Venegas and Halberg (2012) with minor modifications. Briefly, cells were lysed in
150 100 µL LiAc 0,2M SDS 1% at 75°C for 10min, then mixed with 300 µl 100% EtOH and
151 centrifugated for 3min at 15000g followed by a washing step with 500µL 70% EtOH and
152 centrifugated for 3min at 1500g. Finally, total DNA was resuspended in 100µL TE (Tris 10mM pH8;
153 EDTA 1mM) and 1µL of a 10-fold dilution used as template for RT-qPCR measurement. The
154 GenBank accession numbers and the corresponding primer pairs are summarised in Table S1 (same
155 primer pairs used for gene expression analysis). Real-time qPCR reactions were performed using a
156 Mx3000P QPCR System (Agilent, Stratagene) and the Brilliant III Ultra-Fast SYBR® Green QPCR
157 Master Mix with Low ROX (Agilent, Stratagene) according to the manufacturer's instructions. The
158 programme used was: one cycle at 95°C for 3 min and then 40 amplification cycles at 95°C for 20
159 sec and 60°C for 20 sec. For each sample, the mitochondrial DNA copy-number (MtDNA copy

160 number) was determined by comparing the abundance of a single-copy nuclear gene (*TFBI*)
 161 relatively to that of the mitochondrially-encoded gene *COX2* using the following formula: MtDNA
 162 copy number = $(E_{TFBI})^{Ct-TFBI} / (E_{target})^{Ct-target}$. For each condition, the mean MtDNA copy number and
 163 the associated standard error ($n = 3$) were determined. The measured amplification efficiencies were
 164 1.99 and 1.95 *TFBI* and *COX2* genes, respectively. The gene-specific primers used for real time RT-
 165 PCR assays in yeast are:

Gene	Accession #	Direction	Sequence
<i>TFC6</i>	NM_001180670.1	Forward primer	5'-GCTCCCCAGGGTCAAGTCTA-3'
		Reverse primer	5'-GCCAGTGGATACCTCTGCAT-3'
<i>TFBI</i>	NM_001180619.3	Forward primer	5'-CGGTGGCTTCATCGGAAAAC-3'
		Reverse primer	5'-TTGCCTCGTACAACCTGGGTC-3'
<i>RMD8</i>	NM_001180013.1	Forward primer	5'-GGCCGCTGGATGAACAAGAT-3'
		Reverse primer	5'-TCCCTCATTGCCACGTACAG-3'
<i>COX2</i>	NC_027264.1	Forward primer	5'-TGGTGAAACTGTTGAATTTGAATC-3'
		Reverse primer	5'-CATGACCTGTCCCACACAAC-3'
<i>ATP8</i>	NC_027264.1	Forward primer	5'-ATGCCACAATTAGTTCCATTTTATT-3'
		Reverse primer	5'-CTAGATACATATAATCTTAAGATCATAGGT-3'

166

167 2.5. Miscellaneous Procedures.

168 For mitochondrial enzyme assays and membrane potential analyses, mitochondria were prepared by
 169 the enzymatic method [25] from cells grown until middle exponential phase ($3-4 \times 10^7$ cells/mL) in
 170 rich galactose medium. Previously described procedures were used to measure oxygen consumption
 171 and ATP synthesis rates [26], and mitochondrial ATPase activity [27]. Variations in transmembrane
 172 potential ($\Delta\Psi$) were evaluated using Rhodamine 123 with a SAFAS Monaco fluorescence
 173 spectrophotometer as described [28]. SDS- BN-PAGE analyses were performed according to [29, 30].
 174 Polyclonal antibodies against Atp6 and Atp9 were used after 1:10.000 dilution, and those against
 175 Cox2 (from Molecular Probes) were diluted 1:5.000. Peroxidase-labeled antibodies at 1:10.000
 176 dilution and the ECL reagent of Amersham International were used to reveal proteins probed by the
 177 primary antibodies.

178

179 2.6. Amino-acid alignments and topology of subunit a mutations.

180 Multiple sequence alignment of α -subunits of various origins was performed using Clustal Omega [31].
181 The topology of the mutations is based on atomic structures of yeast F_o [7, 21]. Geometry
182 Minimization of the Phenix software suite [32] was used to regularize geometries of the models, with
183 500 iterations and 5 macro cycles. The shown figures were drawn using PyMOL molecular graphic
184 system [33] and UCSF ChimeraX [34].

185

186 *2.7. Statistical analysis*

187 At least three biological and three technical replicates were performed for all experiments. The t-test
188 was used for all data sets. Significance and confidence level was set at 0.05.

189

190

191 **3. Results**

192

193 *3.1. Isolation of revertants from the $aW_{126}R$ mutant*

194 Yeast subunit *a* is synthesized as a pre-protein of which the first N-terminal residues are removed
195 during assembly of ATP synthase [35-37]. The tryptophan residue at position 109 of human subunit *a*
196 that is changed into arginine by the m.8851T>C mutation corresponds to aW_{126} in the yeast mature
197 protein. One nucleotide change was introduced at codon 136 (TGA₁₃₆AGA) to convert this tryptophan
198 residue into arginine ($aW_{126}R$) [15]. As reported [15], the $aW_{126}R$ mutation severely impairs the
199 growth of yeast on non-fermentable substrates (e.g. glycerol, ethanol) at both 28°C (see Fig. 1) and
200 36°C owing to defects in the functioning of ATP synthase. Revertants having recovered a good
201 respiratory growth were isolated from forty subclones of the $aW_{126}R$ mutant, to ensure genetic
202 independence of the rescuing mutational alleles (see Materials and Methods). 10^8 cells from each
203 subclone grown in rich 10% glucose were spread on glycerol plates and incubated for two weeks at
204 28°C. Revertants emerged at a 10^{-7} frequency (an average of ten isolates per plate). The gene *ATP6*
205 was entirely sequenced in thirty-two revertants. Three first-site reversions leading to novel amino acid
206 residues at position 126 were identified: AGA₁₃₆ATA ($aR_{126}M$) in two clones, AGA₁₃₆GGA ($aR_{126}G$)
207 in one clone, and AGA₁₃₆AAA ($aR_{126}K$) in two clones (Table 1). Henceforth, these reversions will be
208 designated as $aW_{126}M$ (instead of $aR_{126}M$), $aW_{126}G$ and $aW_{126}K$, to indicate the amino-acid changes
209 relative to the wild type subunit *a* primary sequence. A second-site suppressor, AGA₁₇₉ATA ($aR_{169}M$),
210 was also identified, in four clones. As shown in Fig. 1, representatives of these four revertant strains
211 grew in respiratory medium almost like wild type yeast.

212 No genetic reversion was identified in the *ATP6* gene of the remaining twenty-three sequenced
213 clones. Respiratory competence was preserved after crossing these clones on a minimal glucose
214 medium (W0) to a strain (D273-10B/60) having a wild type nucleus and totally devoid of
215 mitochondrial DNA (ρ^0), which indicated that the suppressors had a mitochondrial origin or were
216 nuclear dominant. The diploid revertant strains were sporulated and respiratory competence
217 segregation in at least six complete tetrads was assessed. In all cases, only 2 spores produced
218 respiratory competent progenies, showing that the suppressors were located in nuclear DNA at a single
219 genetic locus. We didn't analyze further these revertants in the present study.

220

221 *3.2. Oxidative phosphorylation and mitochondrial membrane potential in the revertants*

222 As we reported [15], the *aW*₁₂₆R mutant has a reduced oxidative phosphorylation capacity especially
223 when grown at 36°C with a 90% drop in ATP production relative to the *WT* (60% at 28°C) (Table 2).
224 The mutated ATP synthase accumulates well and assembly intermediates were not detected in BN-gel.
225 The only anomaly is a diminished ratio between F₁F₀ dimers and monomers, especially at elevated
226 temperature where this effect is very pronounced ([15], Fig. 2A). However, formation of cristae -a
227 process that requires ATP synthase dimerization [30]- was not found compromised in the mutant [15].
228 Possibly the mutated ATP synthase keeps *in vivo* the capacity to form dimers but these are fragile and
229 dissociate when subjected to BN-PAGE analysis.

230 As usually observed in yeast ATP synthase defective mutants [12, 15, 38-41], mitochondria
231 from the *aW*₁₂₆R mutant have a diminished content in respiratory complexes, mostly the complex IV
232 ([15], Fig. 2B). Possibly, as discussed [40, 42, 43], complex IV biogenesis is in yeast modulated by
233 the proton transport activity of F₀ *via* the transmembrane potential ($\Delta\Psi$) as means to balance electron
234 transfer and ATP synthesis activities. Consistently, complex IV accumulation was not found
235 diminished in yeast ATP synthase mutants with proton leaks through the F₀ [44-46].

236 We biochemically evaluated the rescuing activity of the suppressors in mitochondria isolated
237 from cells grown at 28 or 36°C in a rich galactose medium, in exactly the same conditions used
238 previously to investigate the consequences of the *aW*₁₂₆R mutation [15]. The electron transfer to
239 oxygen activity was measured using NADH, alone (state 4), after a further addition (75 μ M) of ADP
240 (state 3) and in the presence of the proton ionophore carbonyl cyanide *m*-chlorophenylhydrazone
241 (CCCP) (uncoupled, maximal respiration). Ascorbate/TMPD was used to probe complex IV's activity
242 in isolation. ATP synthesis coupled to NADH oxidation was assayed in the presence of a large excess
243 of external ADP (750 μ M). We additionally monitored changes in the transmembrane electrical
244 potential induced by ethanol and ADP, and evaluated the amounts of complexes III, IV and V by BN-
245 and SDS-PAGE. The previously reported data relative to the *aW*₁₂₆R and *WT* strains are here included
246 for comparison with the revertants.

247

248 3.2.1 In mitochondria from cells grown at 28°C

249 In the conditions used and with Cox2 antibodies, the complexes III and IV from *WT*
250 mitochondria were detected in BN-gels mainly as III₂-IV₂ and III₂-IV₁ oligomers, with the former
251 being more abundant than the latter (Fig. 2B). In *aW*₁₂₆*R* samples, the complexes III dimers associated
252 with one complex IV (III₂-IV₁) were less abundant (40% *vs WT*) whereas those with two complexes
253 IV (III₂-IV₂) almost normally accumulated. Mitochondria from *aW*₁₂₆*K*, *aW*₁₂₆*G*, and *aW*₁₂₆*M* strains
254 had a higher content in III₂-IV₂ (60% to >90%) than *aW*₁₂₆*R* and did not show any decrease in III₂-IV₁,
255 whereas both oligomers were in reduced amounts in *aW*₁₂₆*R* + *aR*₁₆₉*M* (30% and 75%, respectively)
256 (Fig. 2B). Complex V was resolved mainly as dimers and monomers (Fig. 2A). From the gels stained
257 with Coomassie blue, it appeared that it was in similar amounts (80-100%) in the analyzed strains
258 except in *aW*₁₂₆*R* + *aR*₁₆₉*M* strain where a substantial decrease (50%) was observed presumably
259 because of a less efficient assembly/stability as indicated by the presence in BN-gels of free subunit *c*-
260 ring as revealed by Western blotting with subunit *c* (Atp9) antibodies (Fig. 2A). Consistently,
261 mitochondria from the *aW*₁₂₆*K*, *aW*₁₂₆*G*, and *aW*₁₂₆*M* strains respired and produced ATP more
262 efficiently than the original *aW*₁₂₆*K* strain, whereas these activities were not improved by the second-
263 site suppressor mutation *aR*₁₆₉*M* (Table2). However, since the *aW*₁₂₆*R* + *aR*₁₆₉*M* strain has a reduced
264 content in fully assembled ATP synthase compared to *aW*₁₂₆*R*, it can be inferred that with the *aR*₁₆₉*M*
265 change the *aW*₁₂₆*R* one has less detrimental consequences on the ATP synthesis activity of F₁F₀
266 molecules (in cells grown at 28°C). With a similar ATP synthesis and P/O values the *aW*₁₂₆*R* and
267 *aW*₁₂₆*R* + *aR*₁₆₉*M* strains should grow similarly at 28°C, which is not the case: the double mutant
268 grows better than the single one (Fig. 1). This apparent discrepancy is addressed below.

269 We further characterized the influence of the suppressor mutations on oxidative
270 phosphorylation by monitoring changes in transmembrane electrical potential. The mitochondria were
271 first fed with electrons from ethanol, which induced an important fluorescence quenching of
272 Rhodamine 123 in all tested samples (Fig. 3A). This quenching sharply decreases upon a subsequent
273 addition of ADP due $\Delta\Psi$ consumption by the electrogenic exchange of external ADP against matrix-
274 localized ATP, followed by a progressive recovery until most of the added ADP had been transformed

275 into ATP. Consistent with the ATP synthesis assays (see above), the mitochondria with the $aW_{126}R$
276 change, alone or in combination with $aR_{169}M$, took a longer time to recover the membrane potential
277 established before the addition of ADP in comparison to those isolated from the other tested strains.
278 As expected, further additions of KCN and CCCP resulted in a total collapse of $\Delta\Psi$ in all samples.

279

280 *3.2.2. In mitochondria from cells grown at 36°C.*

281 In comparison to mitochondria from the $aW_{126}R$ strain, the rates of ATP synthesis and respiration
282 were several fold increased by all four suppressor mutations (Table 2), ATP synthase recovered a
283 better capacity to form dimers (Fig. 2A), oligomers of complexes III and IV were more abundant (Fig.
284 2B), and the genetically suppressed mitochondria responded much better to ADP in membrane
285 potential analyses (Fig.3A). The $aR_{169}M$ suppressor had less detrimental consequences on the
286 assembly/stability of ATP synthase (Fig. 2A), which likely explains its better suppressor activity at
287 36°C compared to 28°C (Table 2). Despite their beneficial effects, the level of oxidative
288 phosphorylation was substantially diminished with the suppressors in comparison to the *WT*. This
289 indicates that the aW_{126} and aR_{169} residues are important to optimize the functioning of ATP synthase
290 especially at elevated temperature, consistent with their good evolutionary conservation (see below).

291

292 *3.2.2. Influence of the genetic suppressors on the reverse functioning of ATP synthase*

293 The ATP synthase can function reversibly, which is of vital importance in *S. cerevisiae* to maintain an
294 electrical potential across the mitochondrial inner membrane in the absence of oxygen [47]. An easy
295 way to assay ATP synthase reversibility is to measure the rate of ATP hydrolysis in non-osmotically
296 protected mitochondria buffered at pH 8.5, conditions under which this activity is maximal. A large
297 part (85-90%) of it is normally mediated by the F_1 (the main mitochondrial ATPase), and when F_1 and
298 F_0 are properly associated to each other this activity is inhibited by oligomycin because blocking
299 subunit *c*-ring rotation prevents rotation of the central stalk and hence ATP processing in F_1 . As
300 reported [15], oligomycin-sensitive ATP hydrolysis was considerably decreased by the $aW_{126}R$
301 mutation (10-15% vs the *WT*) both at 28°C and 36°C, whereas it was improved (up to 87%) in the
302 revertants (Table 2).

303 We further evaluated the influence of the suppressors on the reverse functioning of ATP
304 synthase by monitoring ATP-induced $\Delta\Psi$ changes in osmotically-protected mitochondria buffered at
305 pH 6.8. The mitochondria were first fed with electrons from ethanol and $\Delta\Psi$ was subsequently
306 collapsed with KCN to remove from F_1 -ATPase its natural inhibitory peptide (IF1), and less than one
307 minute later, well before rebinding of IF1 [48], ATP was added. The ATP is counter-exchanged against
308 ADP present in the matrix and can then be hydrolyzed in F_1 coupled to F_0 -mediated proton transport
309 from the matrix to the IMS. Against a proton gradient the F_1F_0 complex functions slowly, which
310 explains that despite their very poor F_1 -mediated ATP hydrolytic activity the mitochondria from the
311 $aW_{126}R$ strain showed a significant $\Delta\Psi$ variation in response to ATP albeit of smaller amplitude
312 compared to the *WT* ([15], Fig. 3B). ATP induced a larger and more stable fluorescence variation in
313 mitochondria from the revertants, which further illustrates the beneficial effects of the suppressor
314 mutations on the functioning of ATP synthase.

315

316 *3.3 Mitochondrial protein and DNA abundance in cells grown at 28°C*

317 As described above, mitochondria from $aW_{126}R$ and $aW_{126}R + aR_{169}M$ cells grown at 28°C have
318 similar ATP synthesis rate (40% vs *WT*) and P/O values (0.7 vs 1.1). Somewhat intriguingly while the
319 former showed a very poor growth on glycerol the latter grew much better (Fig.1). Previous studies of
320 numerous yeast ATP synthase mutants have revealed, without any exception, that the activity of this
321 enzyme (measured in isolated mitochondria) needs to be reduced by 80% to see obvious respiratory
322 growth defects [14, 49], and it is thus surprising that the respiratory growth of the $aW_{126}R$ strain was
323 so severely compromised at 28°C.

324 We hypothesized that for some reason $aW_{126}R$ cells have a reduced content in mitochondria.
325 To test this hypothesis, we performed several experiments. We first used the DNA-binding 4',6-
326 diamidino-2-phenylindole (DAPI) and mitochondrial potential sensitive MitoTracker-Red CMXRos
327 fluorochromes to visualize nuclear and mitochondrial DNA and the mitochondrial network in log-
328 phase cells after 8h of culture in YPGalA at 28°C. Consistent with their good bioenergetics properties
329 (see above), mitochondria in the three first-site revertants ($aW_{126}K$, $aW_{126}G$ and $aW_{126}M$) showed a
330 well-defined tubular organisation as in the *WT*, whereas the mitochondrial network was somewhat

331 fragmented in the original mutant ($aW_{126}R$) and its second-site revertant ($aW_{126}R + aR_{169}M$) possibly
332 reflecting their inability to express mitochondrial function properly (Fig. 4A) (see [50, 51] for reviews
333 on the links between mitochondrial structure and bioenergetics). There was no apparent indication for
334 a reduction in number in the MtDNA nucleoids in the mutant strains compared to *WT* (Fig. 4A). We
335 further probed by Western blot the cellular content in porin (Por1), a protein of the mitochondrial
336 outer membrane, with the cytosolic protein Ade13 as a reference. No significant difference in the
337 content in Por1 was observed between the analyzed strains (Fig. 4B). We additionally determined the
338 mitochondrial DNA copy number per cell by RT-qPCR using primers specific to the nuclear *TFBI*
339 and mitochondrial *COX2* genes (Fig. 4C). Consistent with previous studies [52], we estimated to about
340 60 the number of mtDNA molecules in the *WT*, and a similar number was scored in the three first-site
341 revertants ($aW_{126}K$, $aW_{126}G$ and $aW_{126}M$). Despite their alteration in mitochondrial function, the
342 $aW_{126}R$ and $W_{126}R + R_{169}M$ strains did not show a reduced content in mitochondrial DNA but a
343 significant 28% increase. We finally estimated the cellular content in *COX2* and *ATP8* transcripts by
344 RT-qPCR. There was no significant difference in *COX2* transcripts between strains, and any of the
345 mutants showed a diminished abundance in *ATP8* transcripts relative to the *WT* (Fig.4D).

346 Taken together, these data preclude that a diminished content of mitochondria in cells and
347 defects in mitochondrial gene expression are responsible for the slow growth phenotype on glycerol of
348 the $aW_{126}R$ strain despite an ATP synthesis rate in isolated mitochondria (40% vs *WT*) well above the
349 threshold value (20%) below which only respiratory growth is normally compromised. At this stage,
350 the sole theoretical explanation we can offer is that the functioning of ATP synthase in $aW_{126}R$ cells is
351 more affected than it is in the assays performed with isolated mitochondria. In these assays, the
352 mitochondria are supplied with large quantities of external ADP to expel rapidly outside the organelle
353 newly synthesized ATP so as to provide the ATP synthase with the highest possible concentration of
354 ADP during the whole course of the experiment. *In vivo*, with possibly a lesser availability in ADP
355 inside the organelle, the rate of ATP synthesis might be less rapid. Whether the strongly reduced
356 capacity of the F_1 to hydrolyze ATP in the $aW_{126}R$ -an effect never observed in the thus far studied
357 yeast *atp6* mutants- is in some way involved in the unusual behaviour of this mutant is an interesting
358 hypothesis.

359

360 3.4. How the *aW*₁₂₆*R* mutation compromises the functioning of *F*₀

361 Within the *F*₀, two hydrophilic clefts connect the two sides of the membrane with the contact zone
362 between the subunit *c*-ring and subunit *a* [5]. During ATP synthesis, protons from the inter-membrane
363 space are transferred to a glutamate residue in subunit *c* (*cE*₅₉) in the cleft on the *p*-side of the
364 membrane and are released into the *n*-side cleft after an almost complete rotation of the ring [3-5, 7, 8,
365 21, 53] (Fig. 5B). The deprotonated subunit *c* monomers are then moved into the *p*-side cleft for a
366 novel loading with protons, which requires an universally conserved arginine residue in subunit *a*
367 (*aR*₁₇₆ in yeast) located on a bended helical segment (*aH*5) that runs along the *c*-ring. The acidic
368 residues *aE*₁₆₂ and *aD*₂₄₄ were recently proposed to be important for the exit of protons from the ring
369 and their transport into the mitochondrial matrix [7, 21].

370 The tryptophan residue of subunit *a* targeted by the m.8851T>C mutation (*aW*₁₀₉ in humans,
371 *aW*₁₂₆ in yeast) is well conserved or replaced by hydrophobic residues (F, L, or V in *A.t.*, *S.p.* and *P.a.*
372 respectively) (Fig. 5A). In the cryo-EM structures of the *S.c.* *F*₁*F*₀ ATP synthase [7, 21], *aW*₁₂₆
373 localizes between helices *aH*4 and *aH*5 at the bottom of the *n*-side cleft near the middle of the
374 membrane (Fig. 4B right panel and E). Its aromatic ring orients towards the *p*-side lipid layer while the
375 indole nitrogen group points into the *n*-side cleft where it forms a hydrogen bond with the carbonyl
376 group of *aY*₁₆₆ (Fig. 5B right panel). Furthermore *aW*₁₂₆ and *aY*₁₆₆ establish a T-shape π - π interaction,
377 which possibly contributes to stabilize the kinked shape of helix *aH*5 (Fig. 4C,D). This topology of
378 *aW*₁₂₆ fits with the well-known importance of tryptophan in structure and function of membrane
379 proteins with a frequent localization at membrane interfaces [54, 55].

380 In our structural modeling of the *aW*₁₂₆*R* change induced by the m.8851T>C mutation the
381 aliphatic moieties of *aW*₁₂₆ and *aR*₁₂₆ largely overlap at the interface of the *n*-side cleft and membrane
382 lipids while the positively charged guanidinium group of *aR*₁₂₆ fully localizes inside the hydrophilic
383 interior of the cleft. *aR*₁₂₆ comes close to the arginine residue *aR*₁₆₉ (*Q*₁₅₂ in humans) positioned in the
384 center of the cleft (Fig. 4C). As a result, an electrostatic and steric hindrance displaces *aR*₁₆₉ towards
385 the *ac*₁₀ interface between *aR*₁₇₆ and *cE*₅₉ (Fig. 4C). In this orientation, *aR*₁₆₉ possibly forms a salt
386 bridge with *cE*₅₉ in the *F*₀ rotational ‘ground state’ as observed in the cryo-EM density map of the *WT*

387 yeast ATP synthase [21]. Consequently, the structural shift of aR_{169} prevents aR_{176} to interact properly
388 with cE_{59} and proton movements within the F_O and rotation of subunit c -ring are impaired, and this
389 explained the lack in ATP synthesis and hydrolysis in mitochondria of the $aW_{126}R$ mutant.

390 With the $aW_{126}M$ and $aW_{126}G$ suppressors the detrimental electrostatic repulsion between
391 aR_{169} and aR_{126} is eliminated, and local hydrophobicity at the original mutated site is restored with
392 aM_{126} or likely with rotation of the aF_{167} side chain in the gap resulting from the presence of a glycine
393 residue at position 126 (Fig. 4D). While a positive charge remains at position 126 with the $aR_{126}K$
394 suppressor, the ammonium group of lysine can easily make a hydrogen bond with the main carbonyl
395 chain of aY_{166} , which keeps away aR_{169} from the c -ring (Fig. 4E). The second-site suppressor $aR_{169}M$
396 (Fig. 4F) further strongly supports our proposal that aR_{169} is responsible for the F_O deficiency in the
397 $aW_{126}R$ mutant because of unfavorable interactions with aR_{176} and/or cE_{59} . Although the $aR_{169}M$
398 change makes the presence of an arginine residue at position 126 less detrimental, the
399 assembly/stability of subunit a was found partially compromised in the double mutant whereas alone
400 the $aW_{126}R$ mutation had no impact on ATP synthase formation and accumulation. This indicates that
401 aR_{169} has in its native conformation a role in stabilizing the n -side cleft.

402

403

404

405 **Conclusion**

406 We previously showed that the tryptophan to arginine change in subunit *a* induced by the pathogenic
407 m.8851T>C mutation (*a*W₁₀₉R in humans, *a*W₁₂₆R in yeast) impairs the activity of yeast F_O without
408 any visible assembly defects and proton leaks through the mitochondrial inner membrane [15]. In light
409 of recently described high-resolution structures of yeast ATP synthase [7, 21], the present suppressor
410 genetics analysis affords a molecular explanation for the detrimental consequences of this mutation in
411 yeast. We provide evidence that it does not directly impairs the functioning of F_O, it does so by
412 inducing an electrostatic repulsion and steric hindrance with an arginine residue (*a*R₁₆₉) located in the
413 center of the *n*-side cleft along which protons are moved between the *c*-ring and the mitochondrial
414 matrix. As a result, *a*R₁₆₉ is displaced towards the two residues (*a*R₁₇₆ and *c*E₅₉) known for a long time
415 to be essential to the activity and of F_O prevent these residues to function properly.

416 If the *a*W₁₂₆ residue is likely not directly involved in the transport of protons across the
417 mitochondrial inner membrane, the suppressor amino acid residues found at position 126 (methionine,
418 glycine, and lysine) only partially restored oxidative phosphorylation especially when yeast was
419 grown at 36°C. As with these residues ATP synthase assembled and accumulated well and the yield in
420 ATP per electron transferred to oxygen was not strongly affected, it can be inferred that the presence
421 of a tryptophan residue at position 126 of subunit *a* optimizes the functioning of yeast F_O, consistent
422 with its good evolutionary conservation. Additionally, our study reveals that *a*R₁₆₉ has a role in
423 stabilizing the *n*-side cleft. These findings highlight the functional importance of the immediate
424 molecular environment of the regions of subunit *a* that are directly involved in proton transport across
425 the mitochondrial membrane.

426 Although yeast *a*R₁₆₉ is conserved in a large number of evolutionary distant species, it is
427 replaced with an electrically neutral glutamine residue in humans (*a*Q₁₅₂) (Fig. 5A). *a*Q₁₅₂ cannot
428 electrostatically trap the essential acidic residue of subunit *c* (*c*E₅₈ in humans) but can impair its
429 interaction with the essential arginine residue of subunit *a* (*a*R₁₅₉). At the very least our study
430 demonstrates that the neuromuscular disorders induced by the m.8851T>C mutation result from a
431 failure in the transport of protons between the subunit *c*-ring and the mitochondrial matrix.

432

433 **Acknowledgements**

434 R.K. was supported by a post-doc fellowship the ANR (Agence Nationale de la Recherche) in
435 J.P.dR.'s lab. K.G. was supported by a post-doc fellowship from the Conseil de la Région Aquitaine.
436 This work was supported by grants from National Science Center of Poland (2016/23/B/NZ3/02098)
437 to R.K., AFM (Association Française contre les Myopathies) to J.-P.dR and D.T.T., and Agence
438 Nationale de la Recherche to A.D. (ANR-12-BSV8-024).

439

440 **Author Contributions**

441 R.K. and F.G. isolated, sequenced and investigated the biochemical properties of the revertants. A.D.
442 performed the structural modeling analyses. K.G performed the experiments described in figure 4. All
443 authors analyzed the data and contributed to the writing of the manuscript. J.-P.dR. designed the
444 research.

445

446 **Legends to figures**

447 Figure 1. *Growth phenotypes*. Fresh 28 °C glucose cultures of the indicated strains were serially
448 diluted and 5 µl of each dilution were dropped on rich glycerol and glucose media. The shown plates
449 were incubated at 28°C or 36°C for 5 days.

450

451 Figure 2. *ATP synthase and respiratory chain complexes*. Mitochondria isolated from yeast strains
452 grown at 28°C and 36°C were solubilized with digitonin (2 g/g protein) and 200 µg of proteins were
453 separated by BN-PAGE in gels containing a 3–10% polyacrylamide gradient. (A) ATP synthases were
454 visualized by western blot after their transfer onto PVDF membrane with antibodies against Atp6
455 (subunit *a*), Atp9 (subunit *c*) or Coomassie blue staining. Dimers (V_2) and monomers (V_1) of ATP
456 synthase, and free subunit *c*-rings are indicated on the left. (B) Complexes III and IV. In the conditions
457 used these complexes are detected as dimers of complex III associated to one (III_2-IV_1) or two
458 complexes IV (III_2-IV_2). These oligomers were revealed by Western blot with antibodies against the
459 Cox2 subunit of complex IV. The gels are representative of two independent experiments. Image-J
460 quantification of the protein complexes is provided.

461

462 Figure 3. *Mitochondrial membrane potential*. Variations in mitochondrial $\Delta\Psi$ were monitored by
463 fluorescence quenching of Rhodamine 123 in mitochondria isolated from the indicated strains grown
464 at the indicated temperatures. The tracings in panel (A) show how the mitochondria fed with electrons
465 from ethanol responded to externally added ADP; those in panel (B) reflect ATP-driven proton-
466 pumping by ATP synthase. The additions were 0.5 µg/mL Rhodamine 123, 75 µg/mL mitochondrial
467 proteins (Mito), 10 µL ethanol (EtOH), 75 µM ADP (panel A), 1 mM ATP (panel B), 2 mM potassium
468 cyanide (KCN), 4 µg/mL oligomycin (oligo), and 4 µM carbonyl cyanide-*m*-chlorophenyl hydrazone
469 (CCCP). The shown tracings are representative of three experiments.

470

471 Figure 4 *Mitochondrial protein and DNA abundance in cells grown at 28°C*. (A) Epifluorescence
472 microscopy of nuclear and mitochondrial DNA and the mitochondrial network in log-phase cells after

473 8h of culture in YPGalA at 28°C, using the DNA-binding 4',6-diamidino-2-phenylindole (DAPI) and
 474 mitochondrial potential sensitive MitoTracker-Red CMXRos fluorochromes. For each strain, more
 475 than 100 cells were observed. Scale bar, 2µm. (B) Abundance of porin relative to Ade13 in total
 476 cellular protein extracts resolved by SDS-PAGE and Western Blot with specific antibodies (mean ±
 477 SD; $n = 3$). (C) Quantification of the copy number of MtDNA per cell in the analyzed strains by RT-
 478 qPCR (mean ± SD; $n = 3$). (D) Expression of the mitochondrial *COX2* and *ATP8* genes relative to
 479 three nuclear genes (*TFC6*, *TFB1* and *RMD8*) quantified by RT-qPCR (mean ± SD; $n = 3$). *
 480 Significant difference vs WT (*: $p < 0.05$, **: $p < 0.01$, ***: $p < 0.001$). [‡] Significant difference vs
 481 $W_{126}R$ condition (^{‡‡‡}: $p < 0.001$).

482

483 Figure 5. How the $aW_{126}R$ mutation compromises proton movements within yeast F_0 . (A) Amino-acid
 484 alignments of α -subunits segments from various mitochondrial origins comprising helices H4, H β and
 485 H5. The shown sequences are from *Homo sapiens* (*H.s.*), *Bos taurus* (*B.t.*), *Xenopus laevis* (*X.l.*),
 486 *Arabidopsis thaliana* (*A.t.*), *Schizosaccharomyces pombe* (*S.p.*), *Podospora anserina* (*P.a.*), *Yarrowia*
 487 *lipolytica* (*Y.l.*) and *Saccharomyces cerevisiae* (*S.c.*). At the top and bottom of the alignment are
 488 numbered the residues of the *H.s.* and mature *S.c.* proteins, respectively. Strictly conserved residues
 489 are in white characters on a red background. The essential R_{176} residue is on a blue background while
 490 similar residues are in red on a white background with blue frames. Residues 126 and 169 mutated in
 491 the here studied yeast strains are on a green background. The secondary structures in the *S.c.* protein
 492 above the alignments are according to [7]. (B) View of the subunit a and the c -ring from the peripheral
 493 stalk (left panel) and following a 90° rotation (right panel) with as indicated the pathway along which
 494 protons are transported from the intermembrane space to the mitochondrial matrix. The p -side and n -
 495 side clefts that connect the two sides of the membrane with subunit c/a interface are materialized as
 496 free lipid area.. The two residues essential (aR_{176} and cE_{59}) for the activity of F_0 , and two others (aD_{244} ,
 497 aE_{162}) important for the exit of protons from the n -side cleft are marked, as well as the two residues
 498 (aW_{126} and aR_{169}) mutated in the strains here studied. (C-F). Views from the rotor (C-E), from the IMS
 499 (D) and from the matrix (F) of the $aW_{126}R$ (C), $aW_{126}G$ (D), $aW_{126}K$ (E) and double $aW_{126}R + aR_{169}M$
 500 changes (F). Three subunits c are display as green tubes with cE_{59} in sticks. The large arrow

501 materializes the putative proton pathway while the dashed arrows indicated rotamer changes of αR_{169}
502 (C) and αF_{167} (D). Hydrogen bonds are drawn as dashed lines. The αW_{126} side chain is shown as
503 yellow and blue ball-and-stick representations while the mutated side chains are in orange sticks
504 but sphere for glycine. The moving side chains are colored in magenta and shown as ball-and-stick
505 representations in αW_{126} while the minimized conformations are in sticks.
506 .
507

508 Table 1.
509 Intragenic suppressors of the *aW*₁₂₆R mutation

Codon change	Amino acid change	Number
Original mutant		
TGA ₁₃₆ AGA	<i>aW</i> ₁₂₆ R	-
Intragenic suppressors		
AGA ₁₃₆ ATA	<i>aW</i> ₁₂₆ M	2
AGA ₁₃₆ GGA	<i>aW</i> ₁₂₆ G	1
AGA ₁₃₆ AAA	<i>aW</i> ₁₂₆ K	2
AGA ₁₇₉ ATA	<i>aR</i> ₁₆₉ M	4

510

511

512
513
514
515

Table 2A. Mitochondrial respiration

Strain	Growth temp. (°C)	Respiration rates nmol O.min ⁻¹ .mg ⁻¹			
		NADH	NADH +ADP	NADH +CCCP	Asc/TMPD + CCCP
WT*	28	279±17	613±12	1081±107	2013±290
W ₁₂₆ R*	28	203±60	347±25	762±15	1036±27
W ₁₂₆ M	28	255±32	517±44	923±163	1153±123
W ₁₂₆ G	28	334±24	644±36	1134±32	1460±61
W ₁₂₆ K	28	332±80	638±14	1117±116	1655±82
W ₁₂₆ R+R ₁₆₉ M	28	217±10	304±10	424±37	563±13
WT*	36	128±4	368±6	734±54	1130±10
W ₁₂₆ R*	36	31±13	55±12	87±7	132±22
W ₁₂₆ M	36	47±4	117±8	192±8	301±41
W ₁₂₆ G	36	62±7	146±34	232±37	355±69
W ₁₂₆ K	36	63±8	170±27	318±45	443±20
W ₁₂₆ R+R ₁₆₉ M	36	52±3	129±7	220±9	319±6

516
517
518

Table 2B. Mitochondrial ATP synthesis/hydrolysis

Strain	Growth temp. (°C)	ATPase activity μmol Pi.min ⁻¹ .mg ⁻¹			ATP synthesis rate nmol Pi.min ⁻¹ .mg ⁻¹			P/O
		- oligo	+ oligo	oligo-sensitive (% WT)	- oligo	+ oligo	oligo-sensitive (% WT)	
		WT*	28	4.48±0.22	0.67±0.11	100	637±18	
W ₁₂₆ R*	28	1.12±0.06	0.50±0.01	16±1	261±14	8.6±1.0	40±3	0.75±0.10
W ₁₂₆ M	28	3.50±0.27	0.50±0.02	79±6	679±22	30±2.0	104±3	1.31±0.17
W ₁₂₆ G	28	2.96±0.10	0.38±0.04	68±2	727±51	23±0.5	113±10	1.12±0.15
W ₁₂₆ K	28	1.54±0.01	0.27±0.03	33±1	686±31	13±1.0	108±9	1.07±0.08
W ₁₂₆ R+R ₁₆₉ M	28	1.78±0.11	1.07±0.05	19±2	206±22	15±2.0	31±5	0.68±0.10
WT*	36	3.55±0.35	0.89±0.01	100	460±10	1.4±1.0	459	1.25±0.03
W ₁₂₆ R*	36	1.02±0.09	0.77±0.13	9±2	41±0.6	9.0±0.3	7±1	0.74±0.21
W ₁₂₆ M	36	3.33±0.88	1.26±0.50	78±24	261±61	7.6±0.8	55±13	2.20±0.76
W ₁₂₆ G	36	2.80±0.26	1.02±0.14	67±7	288±50	3.6±3.7	62±11	2.20±1.04
W ₁₂₆ K	36	3.36±0.35	1.04±0.22	87±10	329±68	6.5±3.4	70±15	1.93±1.30
W ₁₂₆ R+R ₁₆₉ M	36	2.91±0.01	2.12±0.08	30±1	237±30	2.1±0	51±6	1.84±0.36

519
520
521
522
523
524
525
526
527
528
529
530
531
532
533
534

Mitochondria were isolated from cells grown for 5-6 generations in rich galactose medium (YPGalA) at 28°C. Reaction mixes for assays contained 0.15 mg/mL protein, 4 mM NADH, 150 μM ADP (for respiration assays), 750 μM ADP (for ATP synthesis assays), 12.5 mM ascorbate (Asc), 1.4 mM N,N,N,N,-tetramethyl-p-phenylenediamine (TMPD), 4 μM carbonyl cyanide-m-chlorophenyl hydrazone (CCCP), 3 μg/mL oligomycin (oligo). Respiration and ATP synthesis activities were measured using freshly isolated, osmotically protected mitochondria buffered at pH 6.8. For ATPase assays, mitochondria kept at -80°C were thawed and the reaction performed in absence of osmotic protection at pH 8.4. The values reported are averages of triplicate assays ± standard errors. Activities statistically significant comparing to the control mitochondria are in bold (p<0.05).*The data relative to WT and W₁₂₆R strains have been reported [15]; they are here included for comparison with those obtained with the revertants.

535

536 **References**

537

538 [1] M. Saraste, Oxidative phosphorylation at the fin de siècle, *Science*, 283 (1999) 1488-
539 1493.

540 [2] P.D. Boyer, The ATP synthase--a splendid molecular machine, *Annu Rev Biochem*, 66
541 (1997) 717-749.

542 [3] E. Morales-Rios, M.G. Montgomery, A.G. Leslie, J.E. Walker, Structure of ATP synthase
543 from *Paracoccus denitrificans* determined by X-ray crystallography at 4.0 Å resolution, *Proc*
544 *Natl Acad Sci U S A*, 112 (2015) 13231-13236.

545 [4] A. Zhou, A. Rohou, D.G. Schep, J.V. Bason, M.G. Montgomery, J.E. Walker, N.
546 Grigorieff, J.L. Rubinstein, Structure and conformational states of the bovine mitochondrial
547 ATP synthase by cryo-EM, *Elife*, 4 (2015).

548 [5] M. Allegretti, N. Klusch, D.J. Mills, J. Vonck, W. Kuhlbrandt, K.M. Davies, Horizontal
549 membrane-intrinsic alpha-helices in the stator a-subunit of an F-type ATP synthase, *Nature*,
550 521 (2015) 237-240.

551 [6] I.N. Watt, M.G. Montgomery, M.J. Runswick, A.G. Leslie, J.E. Walker, Bioenergetic cost
552 of making an adenosine triphosphate molecule in animal mitochondria, *Proc Natl Acad Sci U*
553 *S A*, 107 (2010) 16823-16827.

554 [7] H. Guo, S.A. Bueler, J.L. Rubinstein, Atomic model for the dimeric FO region of
555 mitochondrial ATP synthase, *Science*, 358 (2017) 936-940.

556 [8] A. Hahn, K. Parey, M. Bublitz, D.J. Mills, V. Zickermann, J. Vonck, W. Kuhlbrandt, T.
557 Meier, Structure of a Complete ATP Synthase Dimer Reveals the Molecular Basis of Inner
558 Mitochondrial Membrane Morphology, *Mol Cell*, 63 (2016) 445-456.

559 [9] E. Morales-Rios, I.N. Watt, Q. Zhang, S. Ding, I.M. Fearnley, M.G. Montgomery, M.J.
560 Wakelam, J.E. Walker, Purification, characterization and crystallization of the F-ATPase
561 from *Paracoccus denitrificans*, *Open biology*, 5 (2015) 150119.

562 [10] N. Bonnefoy, T.D. Fox, Genetic transformation of *Saccharomyces cerevisiae*
563 mitochondria, *Methods Cell Biol*, 65 (2001) 381-396.

564 [11] K. Okamoto, P.S. Perlman, R.A. Butow, The sorting of mitochondrial DNA and
565 mitochondrial proteins in zygotes: preferential transmission of mitochondrial DNA to the
566 medial bud, *J Cell Biol*, 142 (1998) 613-623.

567 [12] M. Rak, E. Tetaud, S. Duvezin-Caubet, N. Ezkurdia, M. Bietenhader, J. Rytka, J.P. di
568 Rago, A yeast model of the neurogenic ataxia retinitis pigmentosa (NARP) T8993G mutation
569 in the mitochondrial ATP synthase-6 gene, *J Biol Chem*, 282 (2007) 34039-34047.

570 [13] A.M. Kabala, J.P. Lasserre, S.H. Ackerman, J.P. di Rago, R. Kucharczyk, Defining the
571 impact on yeast ATP synthase of two pathogenic human mitochondrial DNA mutations,
572 T9185C and T9191C, *Biochimie*, 100 (2014) 200-206.

573 [14] R. Kucharczyk, N. Ezkurdia, E. Couplan, V. Procaccio, S.H. Ackerman, M. Blondel, J.P.
574 di Rago, Consequences of the pathogenic T9176C mutation of human mitochondrial DNA on
575 yeast mitochondrial ATP synthase, *Biochim Biophys Acta*, 1797 (2010) 1105-1112.

576 [15] R. Kucharczyk, M.F. Giraud, D. Brethes, M. Wysocka-Kapcinska, N. Ezkurdia, B. Salin,
577 J. Velours, N. Camougrand, F. Haraux, J.P. di Rago, Defining the pathogenesis of human
578 mtDNA mutations using a yeast model: the case of T8851C, *Int J Biochem Cell Biol*, 45
579 (2013) 130-140.

580 [16] R. Kucharczyk, M. Rak, J.P. di Rago, Biochemical consequences in yeast of the human
581 mitochondrial DNA 8993T>C mutation in the ATPase6 gene found in NARP/MILS patients,
582 *Biochim Biophys Acta*, 1793 (2009) 817-824.

583 [17] R. Kucharczyk, B. Salin, J.P. di Rago, Introducing the human Leigh syndrome mutation
584 T9176G into *Saccharomyces cerevisiae* mitochondrial DNA leads to severe defects in the

585 incorporation of Atp6p into the ATP synthase and in the mitochondrial morphology, *Hum*
586 *Mol Genet*, 18 (2009) 2889-2898.

587 [18] S. Wen, K. Niedzwiecka, W. Zhao, S. Xu, S. Liang, X. Zhu, H. Xie, D. Tribouillard-
588 Tanvier, M.F. Giraud, C. Zeng, A. Dautant, R. Kucharczyk, Z. Liu, J.P. di Rago, H. Chen,
589 Identification of G8969>A in mitochondrial ATP6 gene that severely compromises ATP
590 synthase function in a patient with IgA nephropathy, *Sci Rep*, 6 (2016) 36313.

591 [19] N. Skoczen, A. Dautant, K. Binko, F. Godard, M. Bouhier, X. Su, J.P. Lasserre, M.F.
592 Giraud, D. Tribouillard-Tanvier, H. Chen, J.P. di Rago, R. Kucharczyk, Molecular basis of
593 diseases caused by the mtDNA mutation m.8969G>A in the subunit a of ATP synthase,
594 *Biochimica et biophysica acta. Bioenergetics*, 1859 (2018) 602-611.

595 [20] L. De Meirleir, S. Seneca, W. Lissens, E. Schoentjes, B. Desprechins, Bilateral striatal
596 necrosis with a novel point mutation in the mitochondrial ATPase 6 gene, *Pediatr Neurol*, 13
597 (1995) 242-246.

598 [21] A.P. Srivastava, M. Luo, W. Zhou, J. Symersky, D. Bai, M.G. Chambers, J.D. Faraldo-
599 Gomez, M. Liao, D.M. Mueller, High-resolution cryo-EM analysis of the yeast ATP synthase
600 in a lipid membrane, *Science*, (2018).

601 [22] J. Ye, G. Coulouris, I. Zaretskaya, I. Cutcutache, S. Rozen, T.L. Madden, Primer-
602 BLAST: a tool to design target-specific primers for polymerase chain reaction, *BMC*
603 *Bioinformatics*, 13 (2012) 134.

604 [23] S.A. Bustin, V. Benes, J.A. Garson, J. Hellemans, J. Huggett, M. Kubista, R. Mueller, T.
605 Nolan, M.W. Pfaffl, G.L. Shipley, J. Vandesompele, C.T. Wittwer, The MIQE guidelines:
606 minimum information for publication of quantitative real-time PCR experiments, *Clin Chem*,
607 55 (2009) 611-622.

608 [24] V. Venegas, M.C. Halberg, Measurement of mitochondrial DNA copy number, *Methods*
609 *in molecular biology*, 837 (2012) 327-335.

610 [25] B. Guerin, P. Labbe, M. Somlo, Preparation of yeast mitochondria (*Saccharomyces*
611 *cerevisiae*) with good P/O and respiratory control ratios, *Methods Enzymol*, 55 (1979) 149-
612 159.

613 [26] M. Rigoulet, B. Guerin, Phosphate transport and ATP synthesis in yeast mitochondria:
614 effect of a new inhibitor: the tribenzylphosphate, *FEBS Lett*, 102 (1979) 18-22.

615 [27] M. Somlo, Induction and repression of mitochondrial ATPase in yeast, *Eur J Biochem*, 5
616 (1968) 276-284.

617 [28] R.K. Emaus, R. Grunwald, J.J. Lemasters, Rhodamine 123 as a probe of transmembrane
618 potential in isolated rat-liver mitochondria: spectral and metabolic properties, *Biochim*
619 *Biophys Acta*, 850 (1986) 436-448.

620 [29] U.K. Laemmli, Cleavage of structural proteins during the assembly of the head of
621 bacteriophage T4, *Nature*, 227 (1970) 680-685.

622 [30] P. Paumard, J. Vaillier, B. Coulary, J. Schaeffer, V. Soubannier, D.M. Mueller, D.
623 Brethes, J.P. di Rago, J. Velours, The ATP synthase is involved in generating mitochondrial
624 cristae morphology, *EMBO J*, 21 (2002) 221-230.

625 [31] F. Sievers, A. Wilm, D. Dineen, T.J. Gibson, K. Karplus, W. Li, R. Lopez, H.
626 McWilliam, M. Remmert, J. Soding, J.D. Thompson, D.G. Higgins, Fast, scalable generation
627 of high-quality protein multiple sequence alignments using Clustal Omega, *Molecular*
628 *systems biology*, 7 (2011) 539.

629 [32] P.D. Adams, P.V. Afonine, G. Bunkoczi, V.B. Chen, I.W. Davis, N. Echols, J.J. Headd,
630 L.W. Hung, G.J. Kapral, R.W. Grosse-Kunstleve, A.J. McCoy, N.W. Moriarty, R. Oeffner,
631 R.J. Read, D.C. Richardson, J.S. Richardson, T.C. Terwilliger, P.H. Zwart, PHENIX: a
632 comprehensive Python-based system for macromolecular structure solution, *Acta Crystallogr*
633 *D Biol Crystallogr*, 66 (2010) 213-221.

634 [33] W.L. DeLano, PyMOL molecular graphics system, (2002).

635 [34] T.D. Goddard, C.C. Huang, E.C. Meng, E.F. Pettersen, G.S. Couch, J.H. Morris, T.E.
636 Ferrin, UCSF ChimeraX: Meeting modern challenges in visualization and analysis, *Protein*
637 *science : a publication of the Protein Society*, 27 (2018) 14-25.

638 [35] T. Michon, M. Galante, J. Velours, NH₂-terminal sequence of the isolated yeast ATP
639 synthase subunit 6 reveals post-translational cleavage, *Eur J Biochem*, 172 (1988) 621-625.

640 [36] X. Zeng, W. Neupert, A. Tzagoloff, The metalloprotease encoded by ATP23 has a dual
641 function in processing and assembly of subunit 6 of mitochondrial ATPase, *Mol Biol Cell*, 18
642 (2007) 617-626.

643 [37] C. Osman, C. Wilmes, T. Tatsuta, T. Langer, Prohibitins interact genetically with Atp23,
644 a novel processing peptidase and chaperone for the F₁F₀-ATP synthase, *Mol Biol Cell*, 18
645 (2007) 627-635.

646 [38] S. Marzuki, L.C. Watkins, W.M. Choo, Mitochondrial H⁺-ATPase in mutants of
647 *Saccharomyces cerevisiae* with defective subunit 8 of the enzyme complex, *Biochim Biophys*
648 *Acta*, 975 (1989) 222-230.

649 [39] M.F. Paul, J. Velours, G. Arselin de Chateaubodeau, M. Aigle, B. Guerin, The role of
650 subunit 4, a nuclear-encoded protein of the F₀ sector of yeast mitochondrial ATP synthase, in
651 the assembly of the whole complex, *Eur J Biochem*, 185 (1989) 163-171.

652 [40] M. Rak, E. Tetaud, F. Godard, I. Sagot, B. Salin, S. Duvezin-Caubet, P.P. Slonimski, J.
653 Rytka, J.P. di Rago, Yeast cells lacking the mitochondrial gene encoding the ATP synthase
654 subunit 6 exhibit a selective loss of complex IV and unusual mitochondrial morphology, *J*
655 *Biol Chem*, 282 (2007) 10853-10864.

656 [41] M.J.B. Jean-Francois, H.B. Lukins, S. Marzuki, Post-transcriptional defects in the
657 synthesis of the mitochondrial H⁺-ATPase
658 subunit 6 in yeast mutants with lesions in the subunit 9 structural gene, *Biochimica et*
659 *Biophysica Acta*, 868 (1986) 178-182.

660 [42] I.C. Soto, F. Fontanesi, M. Valledor, D. Horn, R. Singh, A. Barrientos, Synthesis of
661 cytochrome c oxidase subunit 1 is translationally downregulated in the absence of functional
662 F₁F₀-ATP synthase, *Biochim Biophys Acta*, 1793 (2009) 1776-1786.

663 [43] C. Schwimmer, L. Lefebvre-Legendre, M. Rak, A. Devin, P.P. Slonimski, J.P. di Rago,
664 M. Rigoulet, Increasing mitochondrial substrate-level phosphorylation can rescue respiratory
665 growth of an ATP synthase-deficient yeast, *J Biol Chem*, 280 (2005) 30751-30759.

666 [44] Y. Xiao, M. Metz, D.M. Mueller, Partial uncoupling of the mitochondrial membrane by
667 a heterozygous null mutation in the gene encoding the gamma- or delta-subunit of the yeast
668 mitochondrial ATPase, *J Biol Chem*, 275 (2000) 6963-6968.

669 [45] S. Duvezin-Caubet, M. Caron, M.F. Giraud, J. Velours, J.P. di Rago, The two rotor
670 components of yeast mitochondrial ATP synthase are mechanically coupled by subunit delta,
671 *Proc Natl Acad Sci U S A*, 100 (2003) 13235-13240.

672 [46] E. Tetaud, F. Godard, M.F. Giraud, S.H. Ackerman, J.P. di Rago, The depletion of F(1)
673 subunit epsilon in yeast leads to an uncoupled respiratory phenotype that is rescued by
674 mutations in the proton-translocating subunits of F(0), *Mol Biol Cell*, 25 (2014) 791-799.

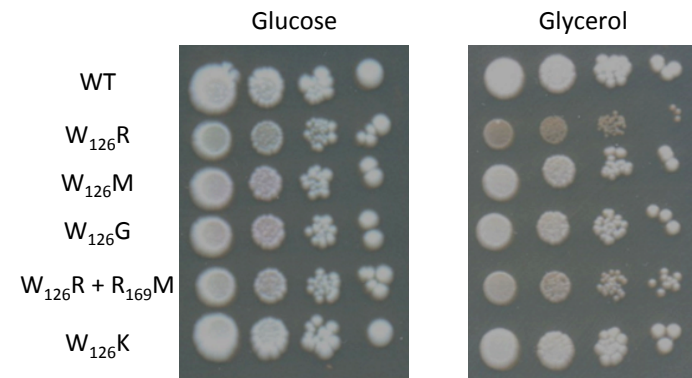
675 [47] L. Lefebvre-Legendre, A. Balguerie, S. Duvezin-Caubet, M.F. Giraud, P.P. Slonimski,
676 J.P. Di Rago, F₁-catalysed ATP hydrolysis is required for mitochondrial biogenesis in
677 *Saccharomyces cerevisiae* growing under conditions where it cannot respire, *Mol Microbiol*,
678 47 (2003) 1329-1339.

679 [48] R. Venard, D. Brethes, M.F. Giraud, J. Vaillier, J. Velours, F. Haraux, Investigation of
680 the role and mechanism of IF1 and STF1 proteins, twin inhibitory peptides which interact
681 with the yeast mitochondrial ATP synthase, *Biochemistry*, 42 (2003) 7626-7636.

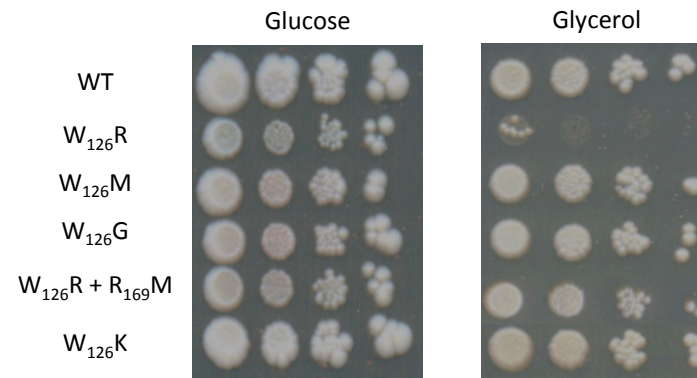
682 [49] A. Mukhopadhyay, M. Uh, D.M. Mueller, Level of ATP synthase activity required for
683 yeast *Saccharomyces cerevisiae* to grow on glycerol media, *FEBS Lett*, 343 (1994) 160-164.

- 684 [50] G. Benard, R. Rossignol, Ultrastructure of the mitochondrion and its bearing on function
685 and bioenergetics, *Antioxidants & redox signaling*, 10 (2008) 1313-1342.
- 686 [51] C. Sauvanet, S. Duvezin-Caubet, J.P. di Rago, M. Rojo, Energetic requirements and
687 bioenergetic modulation of mitochondrial morphology and dynamics, *Semin Cell Dev Biol*,
688 21 (2010) 558-565.
- 689 [52] S. Vijayraghavan, S.G. Kozmin, P.K. Strobe, D.A. Skelly, Z. Lin, J. Kennell, P.M.
690 Magwene, F.S. Dietrich, J.H. McCusker, Mitochondrial Genome Variation Affects Multiple
691 Respiration and Nonrespiration Phenotypes in *Saccharomyces cerevisiae*, *Genetics*, 211
692 (2019) 773-786.
- 693 [53] A. Hahn, J. Vonck, D.J. Mills, T. Meier, W. Kuhlbrandt, Structure, mechanism, and
694 regulation of the chloroplast ATP synthase, *Science*, 360 (2018).
- 695 [54] W.M. Yau, W.C. Wimley, K. Gawrisch, S.H. White, The preference of tryptophan for
696 membrane interfaces, *Biochemistry*, 37 (1998) 14713-14718.
- 697 [55] D.A. Kelkar, A. Chattopadhyay, Membrane interfacial localization of aromatic amino
698 acids and membrane protein function, *Journal of biosciences*, 31 (2006) 297-302.
699

28°C



36°C



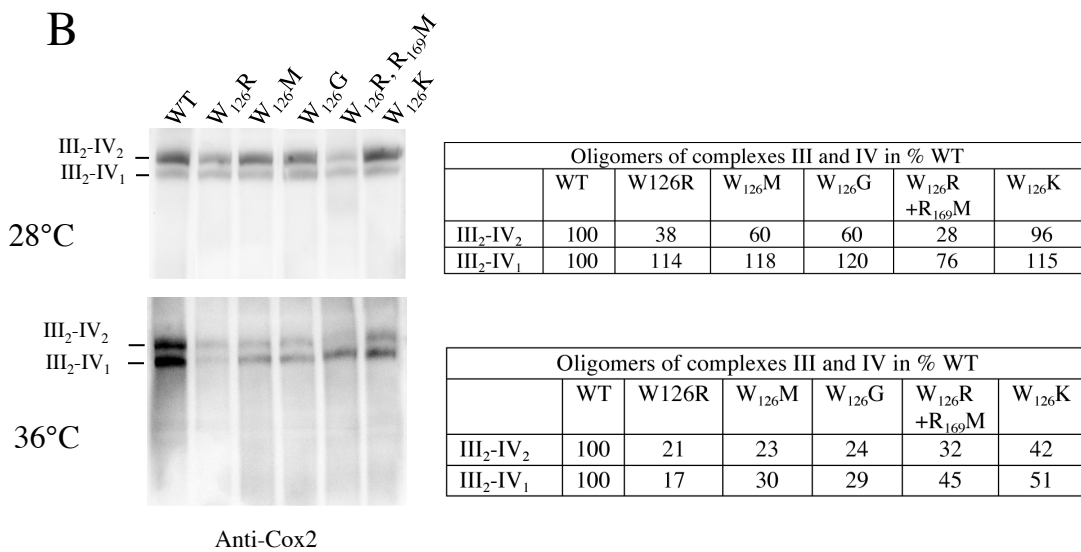
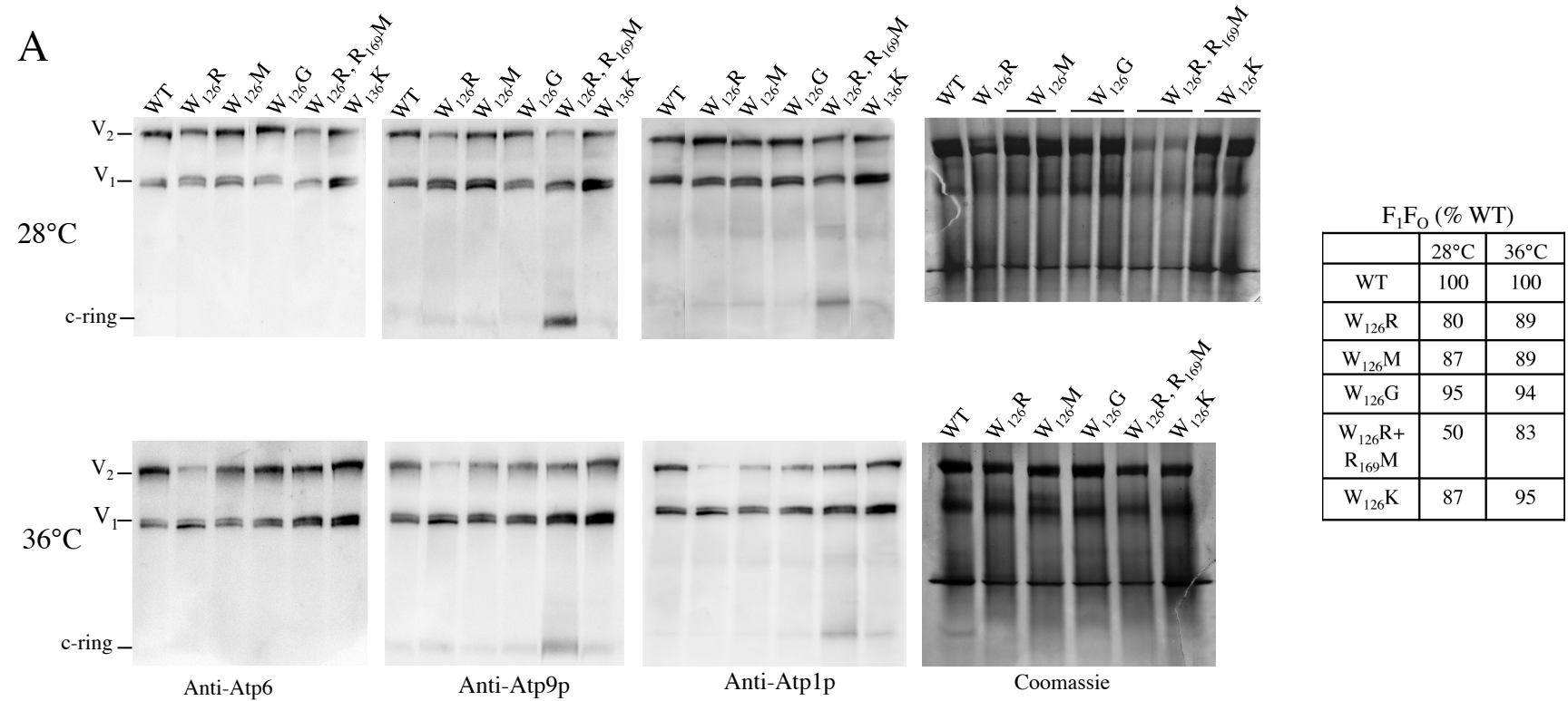
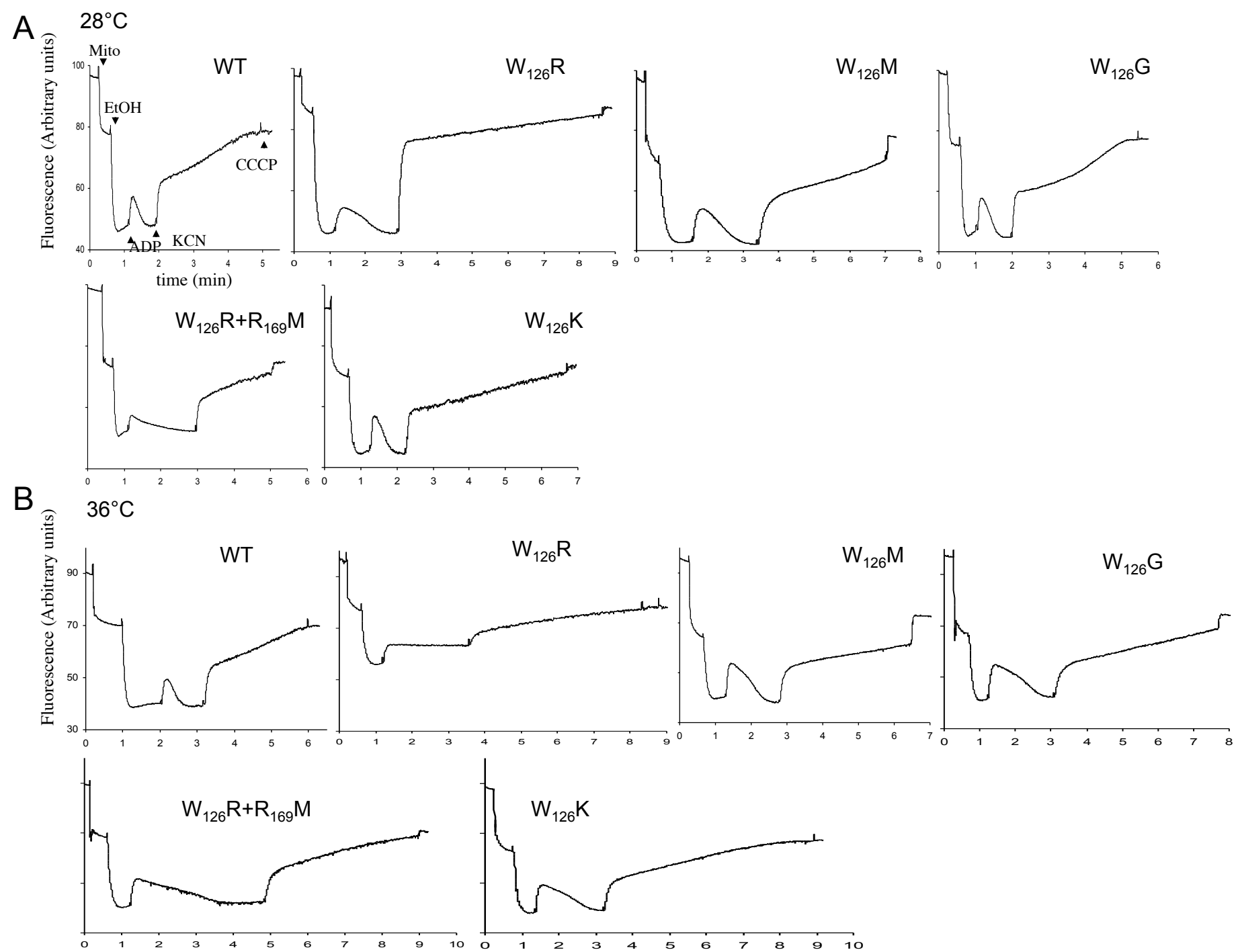


Figure 2



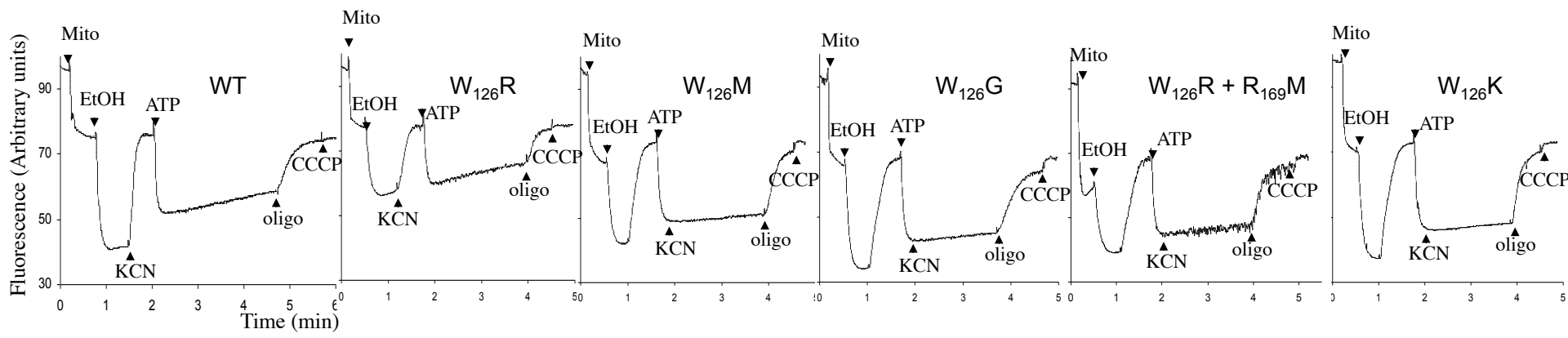


Figure 3B

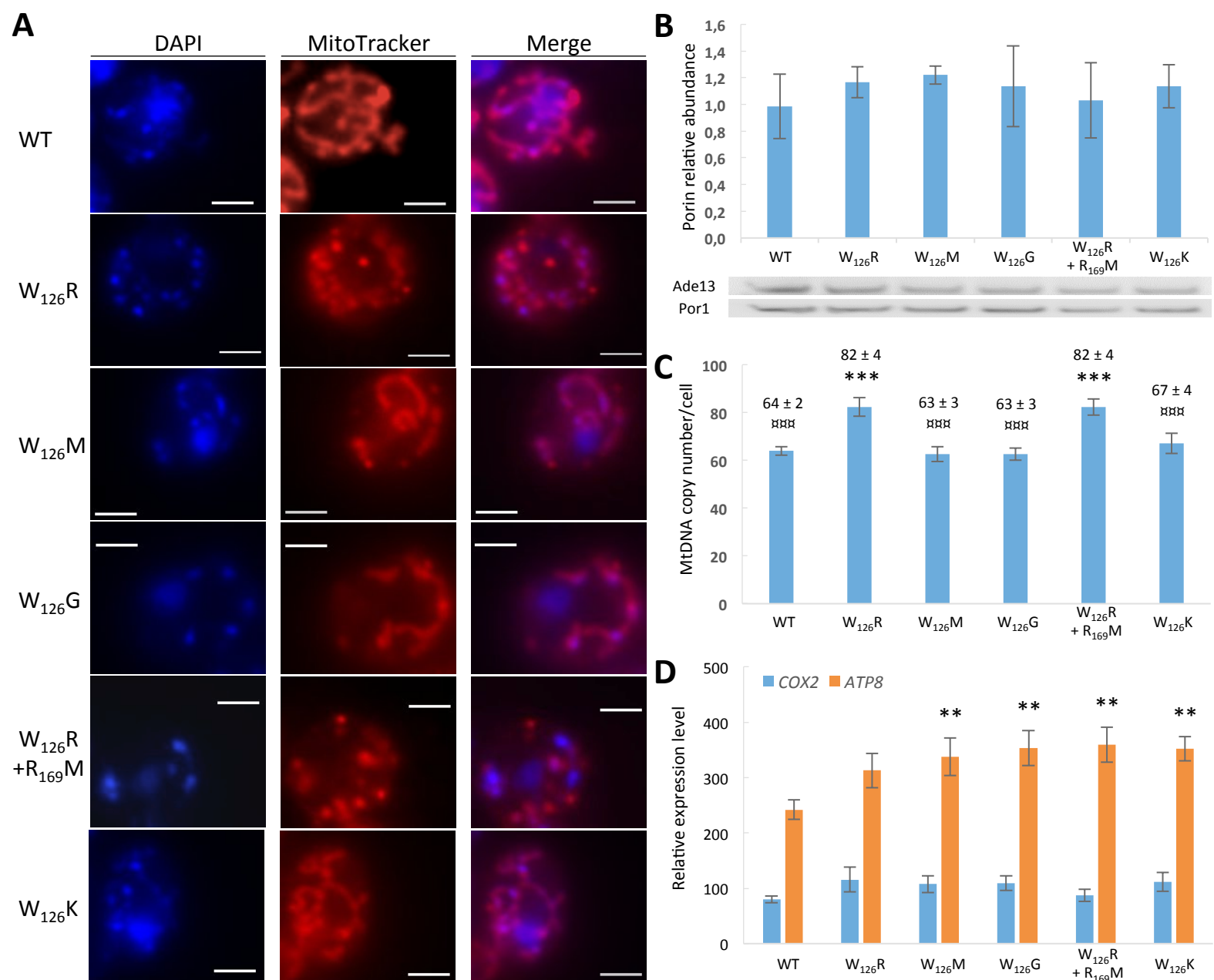


Figure 4

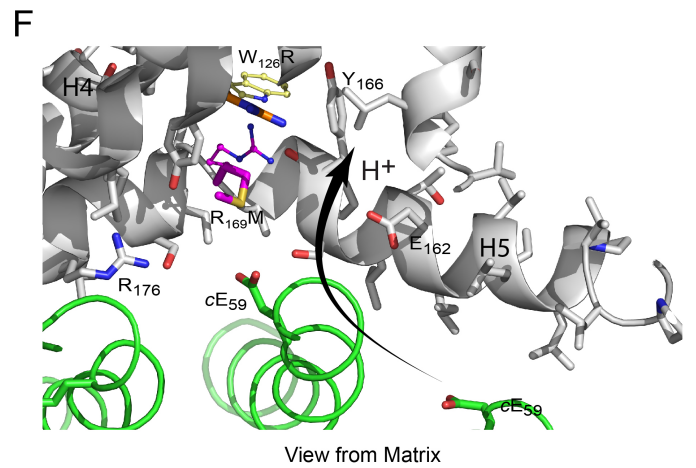
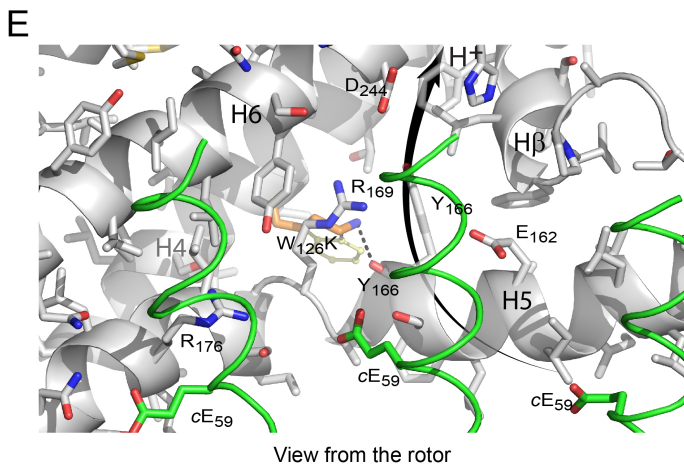
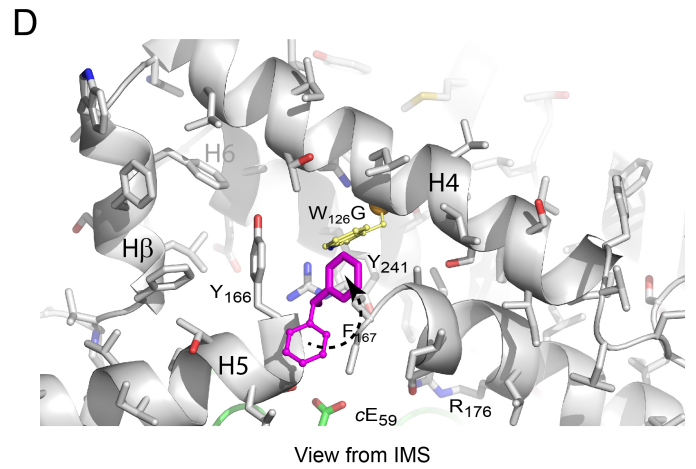
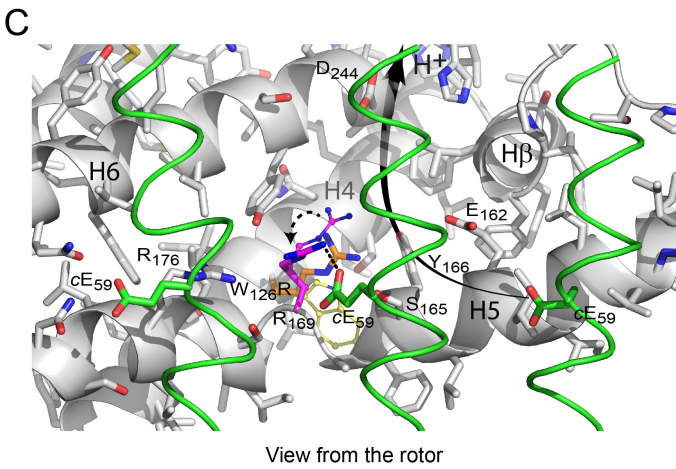
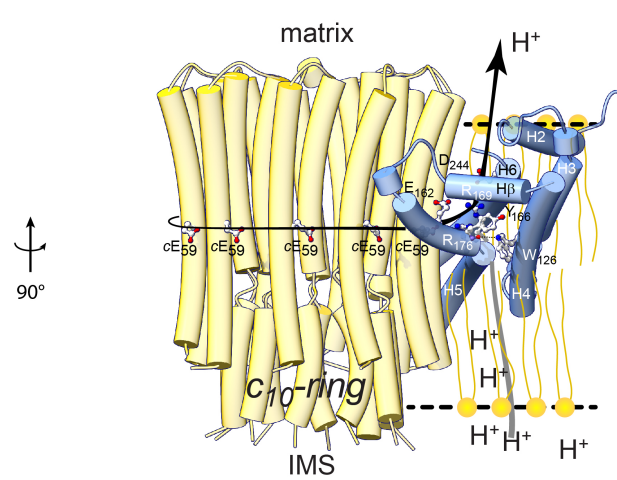
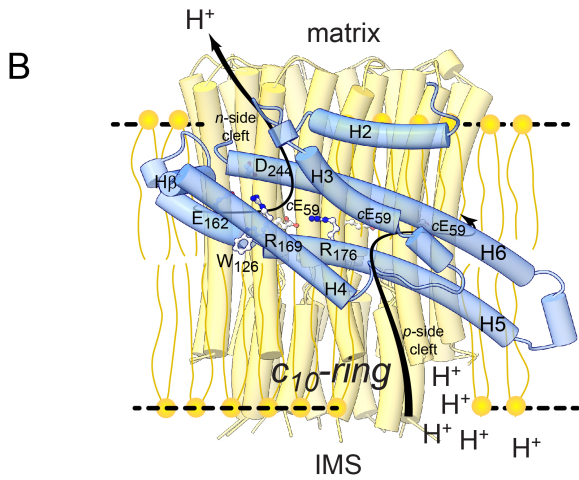
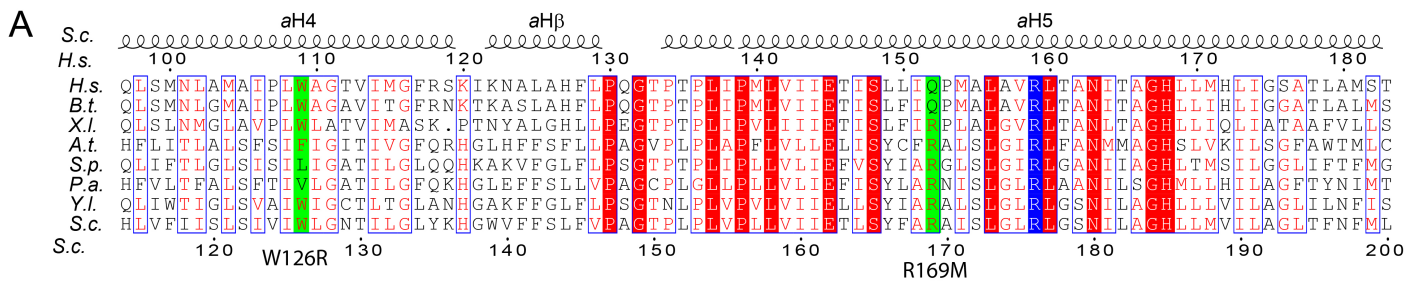


Figure 5